Analysis of Texture Anisotropy Based on Some Gaussian Fields with Spectral Density

Hermine Biermé[1] and Frédéric J.P. Richard[1]

Abstract

In this paper, we describe a statistical framework for the analysis of anisotropy of image texture. This framework is based on the modeling of the image by two kinds of non-stationary anisotropic Gaussian field with stationary increments and spectral density: the extended fractional Brownian field (EFBF) and a specific Gaussian operator scaling field (GOSF), which both correspond to a generalization of the fractional Brownian field. In this framework, we tackle anisotropy analysis using some directional processes that are either defined as a restriction of the image on an oriented line or as a projection of the image along a direction. In the context of EFBF and GOSF, we specify links between the regularity of line and projection processes and model parameters, and explain how field anisotropy can be apprehended from the analysis of process regularity. Adapting generalized quadratic variations, we also define some estimators of the regularity of line and projection processes, and study their convergence to field model parameters. Estimators are also evaluated on simulated data, and applied for illustration to medical images of the breast and the bone.

1 Introduction

Texture analysis is an issue of particular topicality and practical importance in image processing [11, 23]. Texture, which can be roughly considered as a periodic aspect of images, has been modeled using various mathematical approaches ranging from statistical (e.g. Markov random fields [12]) to geometric (e.g. grouplets [24]). Model definitions have also varied depending on texture properties which are focused on. Among those properties, texture anisotropy is one of the most important. It is not

University Paris Descartes, Laboratory MAP5 (CNRS UMR 8145),
45 rue des Saints Pères, 75270 Paris Cedex 06, France.
e-mail: [hermine.bierme,frederic.richard]@parisdescartes.fr.

only common in natural images [24] but also critical for the analysis of images generated in a wide variety of domains, including biometry [16, 17] material science [14], hydro-geology [2], industry [13], or medical imaging [3, 10, 20, 27].

In this paper, we tackle texture analysis from a probabilistic point of view considering the image as a realization of a random field whose properties reflect those of the texture. From this point of view, we deal with the problem of estimating parameters of some anisotropic random field models defined below.

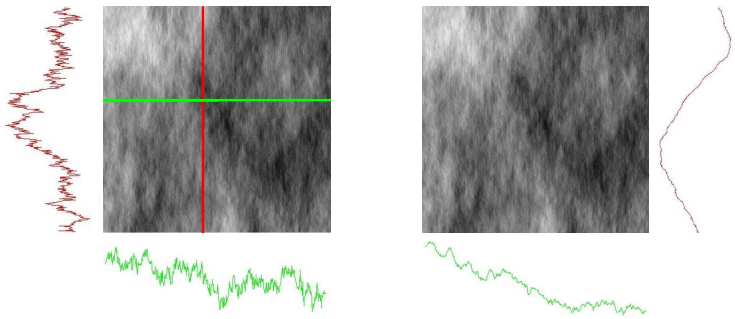

Fig. 1 Oriented analysis of a texture from (a) line processes and (b) projection processes.

Texture anisotropy can be analyzed in a local way by computing oriented differential estimators at each image point [18, 26, 28]. Alternately, anisotropy can be apprehended from processes extracted from image [9, 13, 27], either *line-process* defined by restricting the image on oriented lines of the image domain, or *projection-process* obtained by projecting the image parallel to a given direction ; see the illustration on Fig. 1 and definitions in Eqs. (5) and (7) of Sect. 2. From these processes, anisotropy can be analyzed by looking at regularity variations of processes when the extraction direction changes.

Here, our goal is to set up a statistical framework in which anisotropy can be consistently estimated using line and projection processes.

For defining this framework, we follow the set up of [9] describing d-dimensional Gaussian random fields (with stationary increments) for which the variogram v (see definition in Eq. (4) of Sect. 2) is of the form

$$\forall x \in \mathbb{R}^d, v(x) = \int_{\mathbb{R}^d} \left| e^{ix\cdot\zeta} - 1 \right|^2 f(\zeta) d\zeta, \tag{1}$$

where f is a positive even measurable function called spectral density and satisfying the condition $\int_{\mathbb{R}^d} \left(1 \wedge |\zeta|^2\right) f(\zeta) d\zeta < \infty$. In this set up, we focus on two models defined in dimension $d = 2$.

The first model, referred to as extended fractional Brownian field (EFBF), is defined with a spectral density

$$\forall\, \zeta \in \mathbb{R}^2, f(\zeta) = |\zeta|^{-2h(\arg(\zeta))-2}, \tag{2}$$

where $\arg(\zeta)$ is the direction of the frequency ζ and h is a measurable periodic function defined on the unit sphere $\mathscr{S}^1$ of $\mathbb{R}^2$ and ranging in $[H,M] \subset (0,1)$ with $H = \text{essinf}_{\theta\in S} h(\theta)$ and $M = \text{esssup}_{\theta\in S} h(\theta)$. The fractional Brownian field, which is isotropic, is a particular case of EFBF obtained when function h is almost everywhere constant.

The second model, which can be seen as a Gaussian operator scaling field [2, 5] (GOSF), is defined with

$$\forall\, \zeta = (\zeta_1, \zeta_2) \in \mathbb{R}^2, f(\zeta) = \left(\zeta_1^2 + \zeta_2^{2a}\right)^{-\beta}, \tag{3}$$

where $\beta = H_1 + (1+1/a)/2$ and $a = H_2/H_1$ for some $0 < H_1 \leq H_2 < 1$. The fractional Brownian field is a particular GOSF obtained when $H_1 = H_2$.

Since their spectral density depends on spectral direction, previous models are both anisotropic. Their anisotropy is characterized by model parameters, which are the directional Hurst index h for EFBF and constants H_1 and H_2 for GOSF. Hence, characterizing the anisotropy of these fields reduces to estimating their parameters. In the sequel, we specify links between the regularity of line and projection processes and model parameters, and explain how field anisotropy can be apprehended from the analysis of process regularity. Adapting generalized quadratic variations, we also define some estimators of the regularity of line and projection processes, and study their convergence to field model parameters.

2 Main Properties

2.1 Random fields

Let $(\Omega, \mathscr{A}, \mathbb{P})$ be a probability space. A d-dimensional random field X is a map from $\Omega \times \mathbb{R}^d$ into $\mathbb{R}$ such that $X(\cdot, y) := X(y)$ is a real random variable on Ω for all $y \in \mathbb{R}^d$. When $d = 1$, X is rather called a random process. A random field is Gaussian if any finite linear combination of its associated random variables is a Gaussian variable. A centered Gaussian field X is characterized by its covariance function: $(y,z) \mapsto \text{Cov}(X(y), X(z))$. A field X has stationary increments if laws governing fields $X(\cdot + z) - X(z)$ and $X(\cdot) - X(0)$ are the same for all $z \in \mathbb{R}^d$. The law of a centered Gaussian field X with stationary increments is characterized by its variogram, defined by

$$\forall y \in \mathbb{R}^d,\ v(y) = \mathrm{e}((X(y) - X(0))^2). \tag{4}$$

Gaussian fields with stationary increments and variogram of the form (1) will be referred to as Gaussian fields with spectral density. The EFBF and GOSF defined by Eq. (2) and (3) in introduction are two examples of these fields. From now on, we consider random fields for $d = 2$, corresponding to 2-dimensional images.

2.2 Line and projection processes

We now define line and projection processes which can be extracted from a two dimensional field X.

Definition 0.1. A line process $\mathscr{L}_{t_0,\theta}X$ is the restriction of a field X on a line identified by a point t_0 and a direction θ of $\mathbb{R}^2$:

$$\forall t \in \mathbb{R}, \mathscr{L}_{t_0,\theta}X(t) = X(t_0 + t\theta). \tag{5}$$

We will specifically denote by $\mathscr{L}_\theta X$ the process on the line oriented in direction θ and passing through the origin.

Interestingly, if X is a Gaussian field with spectral density f, the process $\mathscr{L}_{t_0,\theta}X$ is also Gaussian with spectral density [3]

$$\forall v \in \mathbb{R},\ f_{L,\theta}(v) = \int_{\mathbb{R}} f(\xi\theta^\perp + v\theta)d\xi. \tag{6}$$

Definition 0.2. A projection process $\mathscr{P}_\theta X$ of a field X is a windowed Radon transform of a field X in a direction θ of $\mathbb{R}^2$. Given a window function ρ of the Schwartz class such that $\int_{\mathbb{R}} \rho(\gamma)d\gamma = 1$, it is defined as the projection of X along lines oriented in the direction $\theta^\perp$ through the window ρ

$$\forall t \in \mathbb{R}, \mathscr{P}_\theta X(t) = \int_{\mathbb{R}} X(s\theta^\perp + t\theta)\rho(s)ds, \tag{7}$$

If X is a Gaussian field with spectral density f, the projection process is also Gaussian with spectral density

$$\forall v \in \mathbb{R},\ f_{P,\theta}(v) = \int_{\mathbb{R}} f(\xi\theta^\perp + v\theta)\,|\widehat{\rho}(\xi)|^2 d\xi, \tag{8}$$

where f is the spectral density of X.

2.3 Process regularity

For the description of the regularity of a d-dimensional random field, we recall the usual definition of Hölder exponents. For $T > 0$, sample paths of X satisfy a uniform Hölder condition of order $\alpha \in (0,1)$ on $[-T,T]^d$ if there exists a positive random variable A with $\mathbb{P}(A < +\infty) = 1$ such that a.s.

$$\forall y, z \in [-T,T]^d,\ |X(y) - X(z)| \leq A|y - z|^\alpha. \tag{9}$$

This equation gives a lower bound for the Hölder regularity of a field. The critical Hölder exponent β of a field (if it exists) is defined as the supremum of α for which

the Hölder condition (9) holds when it equals the infimum of α for which the Hölder condition (9)does not hold [9]. From an image point of view, the critical Hölder exponent of a field is related to the roughness of the texture: the rougher the texture is, the smaller the field regularity is.

For Gaussian fields with spectral density, the Hölder regularity can be characterized from the local behavior of the variogram around 0 or from the asymptotic behavior of the spectral density at high-frequencies [7, 9].

Proposition 0.1. *Let X be a d-dimensional Gaussian field with spectral density f and variogram v.*
(a) Let $0 < \alpha \leq \gamma < 1$. If there exist $A, B_1, B_2 > 0$ and a positive-measure subset E of the unit sphere $\mathscr{S}^{d-1}$ of $\mathbb{R}^d$ such that for almost all $\xi \in \mathbb{R}^d$,

$$(i)\ \ |\xi| \geq A \Rightarrow |f(\xi)| \leq B_1 |\xi|^{-2\alpha-d};$$
$$(ii)\ |\xi| \geq A \text{ and } \frac{\xi}{|\xi|} \in E \Rightarrow |f(\xi)| \geq B_2 |\xi|^{-2\gamma-d};$$

then, there exist $\delta > 0$ and $C_1, C_2 > 0$ such that for all $y \in \mathbb{R}^d$,

$$(iii)\ |y| \leq \delta \Rightarrow C_1 |y|^{2\gamma} \leq v(y) \leq C_2 |y|^{2\alpha}$$

(b) If Condition (iii) holds for any α, γ with $0 < \alpha \leq \beta \leq \gamma < 1$ then β is the critical Hölder exponent of X.

Let us notice that for random processes, we can use a definition of the Hölder regularity which holds for $\beta \geq 1$ [7, 9]. Similarly to Proposition 0.1, this extended Hölder regularity is also characterized by a behavior of the variogram around 0 or an asymptotic decay of the spectral density [7, 9].

We now state a theorem concerning the regularity of line processes associated to Gaussian fields with stationary increments.

Theorem 0.1. *(a) Let X be a 2-dimensional Gaussian field with stationary increments and assume that the line processes of X have Hölder exponents in all directions. Then, Hölder exponents of line processes are the same in all directions, except possibly in one direction where it is higher than in other directions.*
(b) In the particular case of EFBF with spectral density defined as in Eq. (2), Hölder exponents of line processes are equal to $H = \operatorname{essinf}_{\theta \in S} h(\theta)$ whatever their direction.
(c) In the particular case of GOSF with spectral density defined as in Eq. (3), Hölder exponents of line processes are equal to H_1 in all direction except in direction $(0,1)$ where it is equal to H_2.

Proof. Proofs of parts (a) of Theorem 0.1 can be found in [9, 13]. The part (b) and (c) were demonstrated in [3, 9] using Proposition 0.1. Essentially, in the case EFBF, the spectral density $f_{L,\theta}$ of a line process (see Eq. (5)) always satisfies conditions (i) and (ii) of Proposition 0.1 for $\beta = H = \operatorname{essinf}_{\theta \in S} h(\theta)$, whereas in the case of GOSF, it checks those conditions for $\beta = H_2$ in direction $(0,1)$ and for $\beta = H_1$ in all other directions.

As stated by Theorem 0.1, the anisotropy of a Gaussian field with stationary increments has a specific display on the regularity of line processes. In some cases (e.g. EFBF), the anisotropy is simply not observable from line processes whose regularity does not vary according to direction. In other cases (e.g. GOSF), it is only observable in a single privileged direction where the regularity of line process is different from the others. In any cases, there can be at most one direction where the regularity of the line process varies.

Theorem 0.1 also implies that the anisotropy of EFBF and GOSF cannot be analyzed in the same way: whereas the line processes are useless to capture the anisotropy of EFBF, they can help enhancing a privileged direction of GOSF.

Next, we state a theorem about the regularity of the projection processes of EFBF.

Theorem 0.2. *Let X be an EFBF with spectral density defined as in Eq. (2). The Hölder regularity of the projected field $\mathscr{P}_\theta X$ is equal to $h(\theta)+1/2$ for all directions θ of $\mathbb{R}^2$.*

Proof. It was proved in [9] by checking asymptotic conditions on the spectral density of projection processes.

According to this theorem, the anisotropy of an EFBF is observable in projection processes since their regularity is directly related to the directional function h. Hence, projection processes are better suited than line processes for the characterization of EFBF anisotropy.

3 Parameter estimation

In the previous section, we state several theorems showing that parameters of EFBF and GOSF are linked to the regularity of either line or projection processes extracted from the field. Therefore, the problem of estimating the parameters of these fields eventually reduces to the problem of estimating the regularity of several processes. Moreover, the line and projection processes of EFBF and GOSF are Gaussian with stationary increments and can be seen as generalizations of fractional Brownian motions (fBm). Hence, the regularity of these processes can be estimated using techniques developed for the estimation of the regularity parameter of a fBm (Hurst index).

There are numerous estimators of the Hurst index in the literature (see [1] for a survey). Here, we focus on generalized quadratic variations [7, 15, 19] and show how they can be adapted to the estimation of EFBF and GOSF parameters.

3.1 Generalized quadratic variations

Let Y be a Gaussian process with stationary increments and spectral density f, and $\left\{Y\left(\frac{k}{N}\right); 0 \leq k \leq N\right\}$ be an observed sequence of Y. Let us consider the stationary

sequence formed by second-order increments of Y with step $u \in \mathbb{N} \setminus \{0\}$

$$\forall\, p \in \mathbb{Z},\, Z_{N,u}(Y)(p) = Y\left(\frac{p+2u}{N}\right) - 2Y\left(\frac{p+u}{N}\right) + Y\left(\frac{p}{N}\right). \tag{10}$$

Generalized quadratic variations of Y of order 2 are then given by

$$V_{N,u}(Y) = \frac{1}{N-2u+1} \sum_{p=0}^{N-2u} \left(Z_{N,u}(Y)(p)\right)^2. \tag{11}$$

By stationarity of increments, we have $\mathbb{E}(V_{N,u}(Y)) = \mathbb{E}((Z_{N,u}(Y)(0))^2)$. Besides, according to [7], as N tends to $+\infty$,

$$\mathbb{E}(V_{N,u}(Y)) \sim c_H N^{-2H} u^{2H},$$

for some $c_H > 0$, whenever the spectral density f satisfies $f(\xi) \sim_{|\xi|\to+\infty} c|\xi|^{-2H-1}$, with $H \in (0,2)$ and $c > 0$. Thus, we can intuitively define an estimator of H as

$$\widehat{H}_N = \frac{1}{2\log(2)} \log\left(\frac{V_{N,2}(Y)}{V_{N,1}(Y)}\right). \tag{12}$$

In [7, 15], the convergence of this estimator to H with asymptotic normality was demonstrated for $H \in \left(0, \frac{7}{4}\right)$ under some appropriate assumptions on either the variogram of Y or on its spectral density.

3.2 Convergence results

For the estimation of parameters of EFBF or GOSF, we apply generalized quadratic variations to processes extracted from the field and define estimators by comparing variations at different scales as in Eq. (12). In this way, we set line-based estimators $h_N^L(\theta)$ and projection-based estimators $h_N^P(\theta)$

$$\forall\, \theta,\, h_N^L(\theta) = \frac{1}{2\log(2)} \log\left(\frac{V_{N,2}(\mathscr{L}_\theta X)}{V_{N,1}(\mathscr{L}_\theta X)}\right) \tag{13}$$

$$\forall\, \theta,\, h_N^P(\theta) = \frac{1}{2\log(2)} \log\left(\frac{V_{N,2}(\mathscr{P}_\theta X)}{V_{N,1}(\mathscr{P}_\theta X)}\right), \tag{14}$$

where $\mathscr{L}_\theta X$, $\mathscr{P}_\theta X$, and $V_{N,u}(Y)$ are defined by Eqs. (5), (7) and (11), respectively. In what follows, we state several theorems concerning the convergence of these estimators.

Let us start with the estimation of parameters of an EFBF.

Theorem 0.3. *Let X be an EFBF with spectral density defined as in Eq. (2), and θ be a direction in the unit sphere $\mathscr{S}^1$. Assume that h is Lipschitz of order $\alpha \in (1/2, 1]$*

on $\mathscr{S}^1$. *Then, almost surely,*

$$\lim_{N\to+\infty}\left(\hat{h}_N^P(\theta)-\frac{1}{2}\right)=h(\theta), \tag{15}$$

and, in law,

$$\lim_{N\to+\infty}\sqrt{N}\left(\hat{h}_N^P(\theta)-\frac{1}{2}-h(\theta)\right)=\mathscr{N}(0,K), \tag{16}$$

for some positive constant K.

Proof. According to Proposition 2.1 of [7], the spectral density of the projection process $\mathscr{P}_\theta X$ satisfies assumptions of Theorem 4.1 of [4] and therefore Section 4.3 of [4] gives the result.

This theorem ensures the consistency of $\hat{h}_N^P$ as an estimator of the directional function h of an EFBF, together with its asymptotic normality. Theorem 0.3 only concerns the convergence of a projection-based estimator obtained in a single direction. In [27], we showed another result on the convergence of combinations of estimators in different directions.

Theorem 0.4. *Let* X *be an EFBF with spectral density defined as in Eq. (2). Let* $\theta_0=(0,1)$ *and* $\theta_0^\perp=(1,0)$. *Assume that* h *is Lipschitz of order* $\alpha\in(1/2,1]$ *on* $\mathscr{S}^1$. *Then, almost surely,*

$$\lim_{N\to+\infty}\left(\hat{h}_N^P(\theta_0)-\hat{h}_N^P(\theta_0^\perp)\right)=h(\theta_0)-h(\theta_0^\perp), \tag{17}$$

and in law,

$$\lim_{N\to+\infty}\sqrt{N}\left(\hat{h}_N^P(\theta_0)-\hat{h}_N^P(\theta_0^\perp)-(h(\theta_0)-h(\theta_0^\perp))\right)=\mathscr{N}(0,K), \tag{18}$$

for some positive constant K.

Proof. This result follows from Theorem 3.1 of [27] under the weaker assumption that h is Lipschitz of order $\alpha\in(1/2,1]$ on $\mathscr{S}^1$ and not continuously differentiable. The proof may be adapted using Theorem 0.3 since it only takes into account correlations between combined estimators, which remain unchanged under this assumption.

This theorem is useful to construct hypothesis tests of anisotropy [27]. In these tests, the hypothesis of field isotropy will be rejected if the statistic

$$\delta_1=|\hat{h}_N^P(\theta_0)-\hat{h}_N^P(\theta_0^\perp)| \tag{19}$$

is above a bound (see Sect. 4). This bound can be computed for any level of confidence using simulated data.

We have also defined another anisotropy test which is based on the statistic

$$\delta_2 = |\max(\hat{h}_N^P(\theta_0), \hat{h}_N^P(\theta_0^\perp)) - \min(\hat{h}_N^L(\theta_0), \hat{h}_N^L(\theta_0^\perp))|. \tag{20}$$

For this test, the isotropy assumption is rejected if δ_2 is above a bound.

Now, let us turn to the estimation of parameters of a GOSF.

Theorem 0.5. *Let X be a GOSF with spectral density defined as in Eq. (3). Let $\theta = (\theta_1, \theta_2)$ be a direction in the unit sphere $\mathscr{S}^1$.*
(a) If $\theta_1 = 0$ (privileged direction), then almost surely

$$\lim_{N\to+\infty} \hat{h}_N^L(\theta) = H_2. \tag{21}$$

otherwise, almost surely,

$$\lim_{N\to+\infty} \hat{h}_N^L(\theta) = H_1. \tag{22}$$

(b) The convergence in law

$$\lim_{N\to+\infty} \sqrt{N}\left(\hat{h}_N^L(\theta) - H\right) = \mathscr{N}(0,K), \tag{23}$$

occurs when $\theta_1 = 0$ with $H = H_2$, when $\theta_2 = 0$ with $H = H_1$, and when $\theta_1 \neq 0$, $\theta_2 \neq 2$ and $a = H_2/H_1 > 2$ with $H = H_1$.
(c) When $a \leq 2$ and $\theta_1 \neq 0$, we only have

$$\mathbb{E}\left(\left(\hat{h}_N^L(\theta) - H_1\right)^2\right) = O_{N\to+\infty}\left(N^{-2(1-1/a)}\right). \tag{24}$$

Proof. See [3].

This theorem ensures the consistency of $\hat{h}_N^L$ as an estimator of the directional constants H_1 and H_2 of an GOSF. In this case, the asymptotic normality of estimators is guaranteed in all directions provided that the rate H_2/H_1 is large enough, *i.e.* the anisotropy is marked enough.

4 Numerical study

The numerical study of estimators is usually done on a set of synthetic realizations of the random field with known parameter values. Therefore, it requires a good (ideally exact) method for the simulation of field realizations. But, the exact simulation of EFBF or GOSF is an open issue we are still working on. Hence, the numerical evaluation of estimators are not completely feasible.

To our knowledge, simulations methods for Gaussian fields with spectral density come down to Fourier methods which generates approximate realizations with properties that may differs from the theoretical ones [7]. There is however an exact method which was proposed by Stein [29] for the simulation of (isotropic) fractional Brownian fields. But it can be hardly extended to the simulation of anisotropic fields such as EFBF or GOSF.

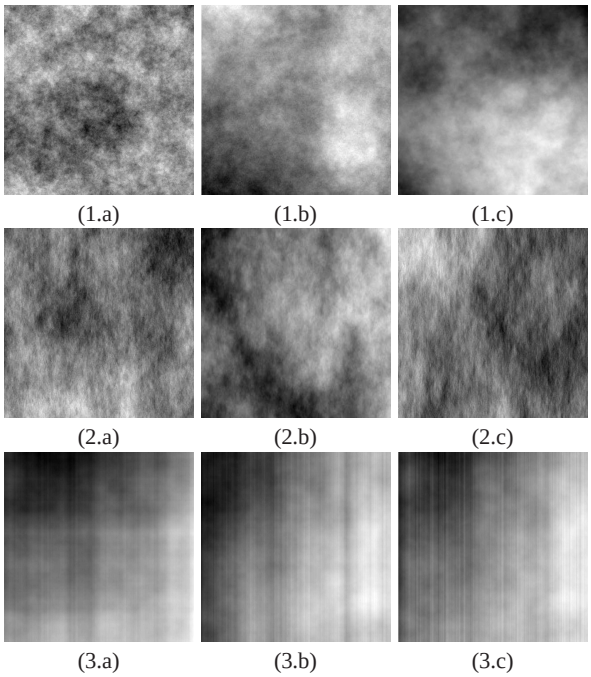

Fig. 2 Exact simulations of fractional Brownian field of increasing Hurst index H (Stein's method): (1.a) $H = 0.3$, (1.b) $H = 0.5$, (1.c) $H = 0.7$. Approximate simulations of extended fractional Brownian field (Turning-Band method): (2.a) $(H_1, H_2) = (0.2, 0.5)$, (2.b) $(H_1, H_2) = (0.5, 0.7)$, (2.c) $(H_1, H_2) = (0.2, 0.7)$. *Ad hoc* simulations of Gaussian operator scaling fields: (3.a) $(H_1, H_2) = (0.7, 0.8)$, (3.b) $(H_1, H_2) = (0.5, 0.8)$, (3.c) $(H_1, H_2) = (0.3, 0.8)$.

Some simulation examples shown on Fig. 2 illustrate some visual features of different fields under studies. Realizations of fractional Brownian fields were obtained using the Stein's method. EFBF were simulated using a turning-band method adapted from [22], which is still under investigation [6]. In these simulations, the spectral density was specified with

$$\forall\, \theta = (\theta_1, \theta_2) \in \mathscr{S}^1, h(\theta) = |\theta_1| H_1 + (1 - |\theta_1|) H_2, \tag{25}$$

for some selected pairs (H_1, H_2) in $(0,1)^2$. The third series of fields are not precisely GOSF. There are just simulations of fields having a variogram of the form $v(x) = c_1 |x_1|^{H_1} + c_2 |x_2|^{H_2}$ and showing a privileged direction.

Our early numerical studies were based on Fourier simulations of EFBF [7, 27]. Here we give some preliminary results based on a turning-band simulations. We simulated sets of EFBF of size (512×512) with spectral density of the form (25), applied line- and projection-based estimators in two directions (horizontal and vertical) to simulations, and then computed biases and standard deviations of estimators. Results are reported in Table 1.

H_1	H_2	$\hat{h}_L^N(\theta_0)$	$\hat{h}_L^N(\theta_0^\perp)$	$\hat{h}_P^N(\theta_0)$	$\hat{h}_P^N(\theta_0^\perp)$
0.2	0.2	0.003±0.003	0.003±0.003	-0.08±0.13	-0.05±0.11
0.5	0.5	0.003±0.003	0.003±0.003	-0.01±0.15	-0.04±0.14
0.7	0.7	0.003±0.003	0.003±0.003	-0.02±0.13	-0.04±0.13
0.2	0.5	0.053±0.003	0.083±0.003	-0.02±0.16	-0.08±0.13
0.2	0.7	0.060±0.005	0.088±0.003	-0.06±0.17	-0.29±0.15
0.5	0.7	0.044±0.004	0.096±0.003	-0.03±0.13	-0.04±0.12

Table 1 Evaluation of line- and projection-based estimators on sets of 100 extended fractional Brownian fields simulations (Turning-Band method) with different Hurst indices (bias±std).

Applied to these simulations, both line-based estimators approximate the regularity $H = \min(H_1, H_2)$, whereas projection-based estimators give an approximation of H_1 or H_2, depending of their direction. Standard deviations of line-based estimators are very small (below 10^{-2}) compared to those of projection-based estimators (above 10^{-1}). This is due to a sub-sampling procedure we apply to projections so as to reduce the bias of projection-based estimators [7]. Biases of line-based estimators are also very small, especially when simulated fields are isotropic ($H_1 = H_2$). However, as the field anisotropy increases, H tends to be overestimated. This might be due either to a simulation artifact or a property of the estimator. Biases of projection-based estimators are reasonably small; most of them are below 10^{-1}. When the anisotropy is large ($H_1 = 0.2$ and $H_2 = 0.7$), the highest directional regularity is however underestimated.

		First test		Second test	
$h(\theta_0)$	$h(\theta_0^\perp)$	δ_1	p	δ_2	p
0.2	0.2	0.01±0.16	94	0.08±0.06	93
0.5	0.5	0.01±0.14	98	0.07±0.05	97
0.7	0.7	0.±0.13	99	0.07±0.05	99
0.2	0.5	0.±0.10	53	-0.08±0.06	39
0.2	0.7	-0.1±0.10	36	-0.28±0.06	32
0.5	0.7	-0.1±0.06	100	-0.12±0.04	100

Table 2 Evaluation anisotropy tests on sets of 100 extended fractional Brownian fields simulations (Turning-Band method) with different Hurst indices (bias±std ; p =percent of realizations considered isotropic).

In Table 2, we present an evaluation of isotropy tests defined with statistics δ_1 and δ_2 given by Eqs. (19) and (20). Observing biases and variances of δ_1 and δ_2 on isotropic simulations, we set rejection bounds for isotropy tests so as to get a level of confidence of 95%. We applied isotropy tests to all simulations and compute the percentage of images considered isotropic in each simulation sets (value p). On isotropic simulations, we observe that tests effectively detect the isotropic cases with a high level of confidence. On anisotropic cases, results show that tests can detect anisotropy only if the anisotropy is marked ($|h(\theta_0) - h(\theta_0^\perp)| > 0.2$). In simulation cases when anisotropy is the largest ($h(\theta_0) = 0.2$ and $h(\theta_0^\perp)| = 0.7$), the risk of

second species (*i.e.* the probability of considering that an anisotropic realization is isotropic) is still high for both tests (around 35%). The lack of sensitivity of tests to anisotropy is mainly due to the large variance of projection-based estimators. We are currently working on the improvement of estimator precision.

5 Applications

We present two applications of the statistical framework described above. In these applications, images are either breast radiographs (mammograms) or bone radiographs, both being used by physicians in clinical routine [21, 27]; see Fig. 3 for illustration.

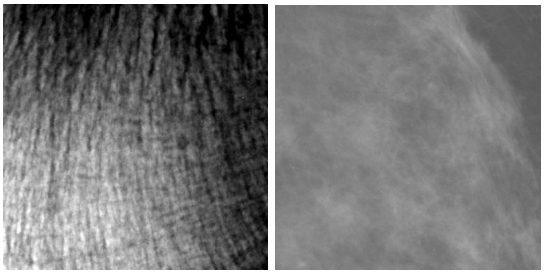

Fig. 3 Regions extracted from (a) a radiography of the calcaneum (a heel bone) and (b) a mammogram (breast radiography).

In [3, 27], we could show on some database that both images are anisotropic. Assuming mammograms to be realizations of EFBF and applying anisotropy tests on them, we obtained that 41 percent of mammograms could be considered as anisotropic with a level of confidence of 95% [27]. This anisotropy can be seen both, on Fig. 4 (b), where horizontal and vertical projection-based estimates are plotted for each mammograms, and on Fig. 4 (c), where the maximum of horizontal and vertical projection-based estimates is plotted against the minimum of horizontal and vertical line-based estimates.

The anisotropy of bone radiographs can be observed on Fig. 5, where couples of line-based estimates in different directions (horizontal, vertical, or diagonals) are plotted for each images. It can be seen that in the vertical direction $\theta_0^{\perp}$, the regularity tends to be higher than in the three other directions; this direction corresponds to the axis of longitudinal trabeculae of the bone. Hence, according to Theorem 0.1, GOSF would be better suited than EFBF for the modeling of bone radiographs.

The anisotropy of mammograms is different from the one of bone radiographs. According to Figs. 4 (a) and (b), it seems not to be detected on lines. Contrarily to bone radiographs, mammograms would be better described by EFBF.

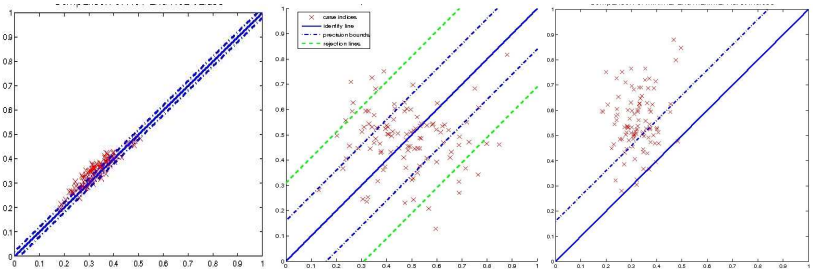

(a) (b) (c)

Fig. 4 Line- and projection-based estimates obtained on 116 full-field digital mammograms (private database, courtesy of P. Bakic and A. Maidment from Univ. of Pennsylvania): comparisons of (a) $h_N^L(\theta_0)$ (abscissa) and $h_N^L(\theta_1)$, (b) $h_N^P(\theta_0)$ and $h_N^P(\theta_1)$, and $\min(h_N^L(\theta_0), h_N^L(\theta_1))$ and $\max(h_N^P(\theta_0), h_N^P(\theta_1))$. [directions:$\theta_0 = (1,0)$ (horizontal), $\theta_0^\perp = (0,1)$ (vertical)].

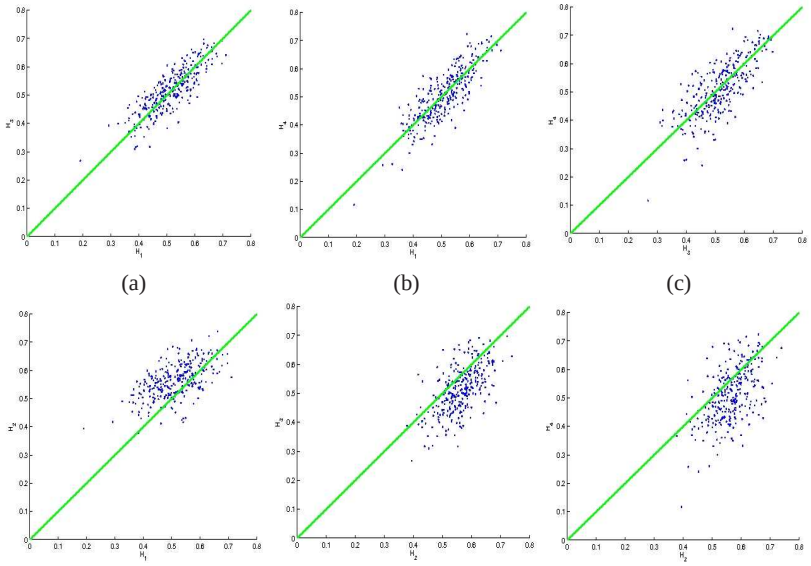

(a) (b) (c)

(d) (e) (f)

Fig. 5 Line-based estimates obtained on 211 calcaneum radiographs (database of Inserm unit U658 [21]): comparisons of (a) $h_N^L(\theta_0)$ (abscissa) and $h_N^L(\theta_1)$ (ordinate), (b) $h_N^L(\theta_0)$ and $h_N^L(\theta_1^\perp)$, (c) $h_N^L(\theta_1)$ and $h_N^L(\theta_1^\perp)$, (d) $h_N^L(\theta_0)$ and $h_N^L(\theta_0^\perp)$, (e) $h_N^L(\theta_0^\perp)$ and $h_N^L(\theta_1)$, and (f) $h_N^L(\theta_0^\perp)$ and $h_N^L(\theta_1^\perp)$. [directions:$\theta_0 = (1,0)$ (horizontal), $\theta_0^\perp = (0,1)$ (vertical), 3: $\theta_1 = (1,1)/\sqrt{2}$ (diagonal), 4: $\theta_1^\perp = (-1,1)/\sqrt{2}$ (diagonal)].

Previous experiments are preliminary steps of a multidisciplinary project which concern the evaluation of (a) breast cancer risk and (b) bone fracture risk due to osteoporosis [8, 25, 27]. In the context of this project, the line and projection estimates

are used as descriptors of image aspect. By combining such descriptors to known clinical risk factors, we aim at improving the evaluation of both risks.

Acknowledgements

This work is part of the research program MATAIM, supported by the Agence Nationale pour la Recherche (ANR-09-BLAN-0029-01) and the Institut National du Cancer (INCA, 2009-1-SHS SP-01-UP5-1).

References

1. J. M. Bardet, G. Lang, G. Oppenheim, et al. Semi-parametric estimation of the long-range dependence parameter: a survey. In *Theory and applications of long-range dependence*, pages 557–577. Birkhauser Boston, 2003.
2. D. Benson, M. M. Meerschaert, B. Bäumer, and H. P. Scheffler. Aquifer operator-scaling and the effect on solute mixing and dispersion. *Water Resour. Res.*, 42:1–18, 2006.
3. H. Biermé, C.L. Benhamou, and F. Richard. Parametric estimation for gaussian operator scaling random fields and anisotropy analysis of bone radiograph textures. In K. Pohl, editor, *Proc. of the International Conference on Medical Image Computing and Computer Assisted Intervention (MICCAI'09), Workshop on Probabilistic Models for Medical Imaging*, pages 13–24, London, UK, september 2009.
4. H. Biermé, A. Bonami, and J. R. León. Central limit theorems and quadratic variations in terms of spectral density. *preprint*, 2010.
5. H. Biermé, M. M. Meerschaert, and H. P. Scheffler. Operator scaling stable random fields. *Stoch. Proc. Appl.*, 117(3):312–332, 2007.
6. H. Biermé, L. Moisan, and F. Richard. A turning-band method for the simulation of anisotropic fractional brownian fields. *in preparation*, 2010.
7. H. Biermé and F. Richard. Estimation of anisotropic gaussian fields through radon transform. *ESAIM:P& S*, 12(1):30–50, 2008.
8. H. Biermé, F. Richard, M. Rachidi, and C.L. Benhamou. Anisotropic texture modeling and applications to medical image analysis. In *ESAIM Proceedings: Mathematical Methods for Imaging and Inverse Problems*, pages 100–122, 2009.
9. A. Bonami and A. Estrade. Anisotropic analysis of some Gaussian models. *J. Fourier Anal. Appl.*, 9:215–236, 2003.
10. B. Brunet-Imbault, G. Lemineur, C. Chappard, et al. A new anisotropy index on trabecular bone radiographic images using the fast Fourier transform. *BMC Med. Imaging*, 5(4), 2005.
11. M.J. Chantler and L.J. Van Gool. Editorial: Special issue on texture analysis and synthesis. *Int. J. Comput. Vis.*, 62(1-2):5–5, April 2005.
12. G. Cross and A. Jain. Markov random field texture models. *IEEE Trans PAMI*, 5(1):25–39, 1983.
13. S. Davies and P. Hall. Fractal analysis of surface roughness by using spatial data. *J. R. Stat. Soc. Ser. B*, 61:3–37, 1999.
14. C. Germain, J. P. Da Costa, O. Lavialle, and P. Baylou. Multiscale estimation of vector field anisotropy application to texture characterization. *Signal Process.*, 83(7):1487–1503, 2003.
15. J. Istas and G. Lang. Quadratic variations and estimation of the local Holder index of a Gaussian process. *Ann. Inst. Henri Poincaré, Prob. Stat.*, 33(4):407–436, 1997.

16. A. Jain, L. Hong, and R. Bolle. On-line fingerprint verification. *IEEE Transactions on Pattern Analysis and Machine Intelligence*, 19:302–314, 1997.
17. X.D. Jiang. On orientation and anisotropy estimation for online fingerprint authentication. *IEEE Trans. Sig. Proc.*, 53(10):4038–4049, 2005.
18. M. Kass and A. Witkin. Analyzing oriented patterns. *Computer Vision, Graphics, and Image Processing*, 37(362–385), 1987.
19. J. T. Kent and A. T. A. Wood. Estimating the fractal dimension of a locally self-similar Gaussian process by using increments. *J. Roy. Statist. Soc. Ser. B*, 59(3):679–699, 1997.
20. G. Lemineur, R. Harba, R. Jennane, et al. Fractal anisotropy measurement of bone texture radiographs. In *First International Symposium on Control, Communications and Signal Processing*, pages 275–278, 2004.
21. E. Lespessailles, C. Gadois, I. Kousignian, J.P. Neveu, P. Fardellone, S. Kolta, C. Roux, J.P. Do-Huu, and C.L. Benhamou. Clinical interest of bone texture analysis in osteoporosis: a case control multicenter study. *Osteoporos. Int.*, 19:1019–1028, 2008.
22. G. Matheron. The intrinsic random functions and their applications. *Adv. in Applied Probab.*, 5(3):439–468, 1973.
23. M. Nielsen, L.K. Hansen, P. Johansen, and J. Sporring. Guest editorial: Special issue on statistics of shapes and textures. *J. Math. Imaging Vis.*, 17(2):87–87, September 2002.
24. G. Peyré. Texture synthesis with grouplets. *IEEE Trans. Pattern Anal. Mach. Intell.*, 32(4):733–746, 2010.
25. M. Rachidi, F. Richard, H. Biermé, E. Lespessailles, C. Chappard, and C.L. Benhamou. Conception of a composite osteoporosis fracture index including bone texture analysis and bone mineral density. In *Proc. of the 18th International Bone Densitometry Workshop IBDW'08*, Foggia, Italy, june 2008.
26. A. Rao and R. Jain. Computerized flow field analysis: Oriented texture fields. *IEEE Trans. Pattern Anal. Mach. Intell.*, 14:693–709, 1992.
27. F. J.P. Richard and H. Biermé. Statistical tests of anisotropy for fractional brownian textures. application to full-field digital mammography. *J. Math. Imaging Vis.*, 36(3):227–240, 2010.
28. C. Shu and R. Jain. Vector field analysis for oriented patterns. *IEEE Trans. Pattern Anal. Mach. Intell.*, 16:946–950, 1994.
29. M. L. Stein. Fast and exact simulation of fractional Brownian surfaces. *J. Comput. Graph. Statist.*, 11(3):587–599, 2002.